Electromagnetic-thermo-mechanical Coupling Behavior of Cu/Si Layered Thin Plate under Pulsed Magnetic Field

Qicong Li[1], Linli Zhu[1*], Haihui Ruan[2*]

[1]Department of Engineering Mechanics, and Key Laboratory of Soft Machines and Smart Devices of Zhejiang Province, Zhejiang University, Hangzhou 310027, China

[2]Department of Mechanical Engineering, The Hong Kong Polytechnic University, Hong Kong, China

[*] Authors to whom correspondence should be addressed; electronic mail: llzhu@zju.edu.cn (Linli Zhu) and haihui.ruan@polyu.edu.hk (Haihui Ruan).

Abstract

Semiconductor-based electronic devices usually work under multi-physics fields rendering complex electromagnetic-thermo-mechanical coupling. In this work, we develop a penalty function method based on a finite element analysis to tackle this coupling behavior in a metal/semiconductor bilayer plate - the representative unit of semiconductor antenna, which receives strong and pulsed electromagnetic signals. Under these pulses, eddy current is generated, of which the magnitude varies remarkably from one plate to another due to the difference in electrical conductivity. In the concerned system, the metal layer generates much larger current, resulting in the large temperature rise and the nonnegligible Lorentz force, which could lead to delamination and failure of the semiconductor-based electronic device. This study provides theoretical guidance for the design and protection of semiconductor-based electronic devices in complex environments.

Keywords: Electromagnetic-thermo-mechanical coupling behavior, Finite element method, Pulse magnetic field, Eddy current, Delamination

1 Introduction

As telecommunication systems advance with high-energy radiofrequency (RF) sources and more efficient antennae, the possible high-power electromagnetic pulses (EMP) lead to the concern of electromagnetic (EM) interference in electronic devices. Intentional EM interference (IEMI) can lead to immediate failure of electronic devices, influencing many key areas, such as transportation, communication, defense, security, medicine, etc. [1-4]. The development of superconducting devices further leads to complex strong electromagnetic environment in devices with the magnetic field close to dozens of Tesla [5, 6]. As the electric, magnetic, thermal, and stress fields could be changed under the electromagnetic interference, the EM protection has become crucial for the application of electronic devices [7-9]. Therefore, it is needed to give insight into the multi-physics coupling behavior quantitatively in analyzing the influence of EM inference in electronic devices [10-12].

The multi-field coupling behavior of electronic system in complex multi-physics environments has been extensively studied in recent decades [13-15]. For the dynamic mechanical response, Horie and Niho [16] developed a finite element method (FEM) to deal with the coupling behavior between the electromagnetic field and structural dynamic responses with large deformation. Tanaka *et al*. [17] proposed a coupling intensity parameter in analyzing the dynamic responses of fusion reactor components through considering the magnetic damping effect on dynamic behavior. Hu *et al.* [18] studied the resonances and stabilities of the current-conducting thin plate in a magnetic field. Zhang *et al*. [19] developed a finite element model to study the nonlinear dynamic response under complex magnetic field. Ghayesh *et al.* [20] applied the modified couple stress theory to explore the size-dependent nonlinear dynamics behavior of the micro-electro-mechanical system (MEMS) with pre-deformable electrode. For the performance of electronic devices. Liu *et al*. [21] investigated the effect of high-power microwave on mobility degradation, avalanche generation, and self-heating in a GaAs high-electron-mobility transistor experimentally and theoretically. Lu *et al*. [22, 23] simulated the electrical-thermal-mechanical coupling behavior in the large-scale 3D interconnects and the high-power RF/microwave circuits using the FEM, which involved cohesive elements and parallel computing.

In recent years, the studies of EM interference behavior in semiconductor-based electronic devices mainly focused on the thermal breakdown caused by EM pulses-induced energy [24-26]. The thermal-related failure behavior in semiconductor-based devices under the EM pulses has been widely investigated in simulations and experiments [27-29]. For example, Dobykin and Kharchenko [27] developed a heat transfer-based mathematical model for thermal damage in semiconductors with one p-n junction under high-energy EM pulses. Zhou *et al*. [30] conducted an experimental study on the destruction of field effect transistor (FET) under high-power microwave (HPM) pulses, and established a two-dimensional analytical model to obtain the thermal breakdown temperature based on experimental data. Zhou *et al*. [31] proposed a generalized thermal damage model in semiconductor devices under EMP to explain the failure mechanisms of device with experimental verification. Zhang *et al*. [32] established a 3D theoretical model to analyze the EMP thermal runaway and to predict the temperature in devices under EMP. Li *et al*. [33] studied the thermal failure behavior in metal-oxide-semiconductor field-effect transistors (MOSFETs) under electro-magnetic pulse through the thermal failure model and the technology computer-aided design (TCAD) simulation, with considering the influences of dissipation performance and electro-thermal coupling effect.

Besides the thermal-related failure behavior in electronic devices under EM pulse, Camp *et al*. [34] investigated the susceptibility of a single microcontroller to EM pulses and ultra-wide band pulses using a statistical procedure. Xi *et al*. [35] investigated the response of a bipolar transistor under a square-shaped EMP and found that the damage energy changed with the input voltage. Ma *et al*. [36] studied the effect of pulse width on the destruction of bipolar transistors and established a typical n+-p-n-n+ bipolar transistor model to analyze the effect of frequency on damage sensitivity. Genender *et al*. [37] proposed an approach to analyze the risk of a system exposed to intentional electromagnetic interference (IEMI), which involves characteristics of physical quantities such as amplitude of electromagnetic field and nonphysical quantities. Shurenkov and Pershenkov [38] analyzed the main cause of semiconductor structure damage and failure mechanisms under different situations. Baek *et al*. [39] investigated the effects of design parameters on the damage rate of a low-noise amplifier (LNA), and analyzed the relationship between damage rate and parameters of LNA.

In this work, we study the coupling behavior of EM, thermal, and stress fields in Si/Cu layered thin plate under EM pulses through the finite element simulation and reveal that the structural integrity could be affected by the cooperation of thermal stress and Lorentz force. In the next section, the governing equations and related finite element formulism for the elastic deformation, Eddy current, and heat conduction are described, as well as the failure criterion for two-layered structure. Section 3 presents the numerical simulations and discussion for single- and multi-pulsed magnetic fields. Section 4 lists conclusions.

2 Theoretical Description

Considering a two-layered thin plate under EM pulses, the equations governing the dynamic response and heat transfer need to be solved through a finite element approach [12, 42, 43]. In this work, the weighted residual method, Hamilton's principle, and variational method are adopted to derive the weak form of governing equations dealing with the multi-field coupling behaviors. The virtual crack closure technique (VCCT) is used to calculate the energy release rate; and the Crank-Niscolson and Newmark methods are employed to solve the variations of displacement and temperature fields, respectively. These formulations are detailed hereunder.

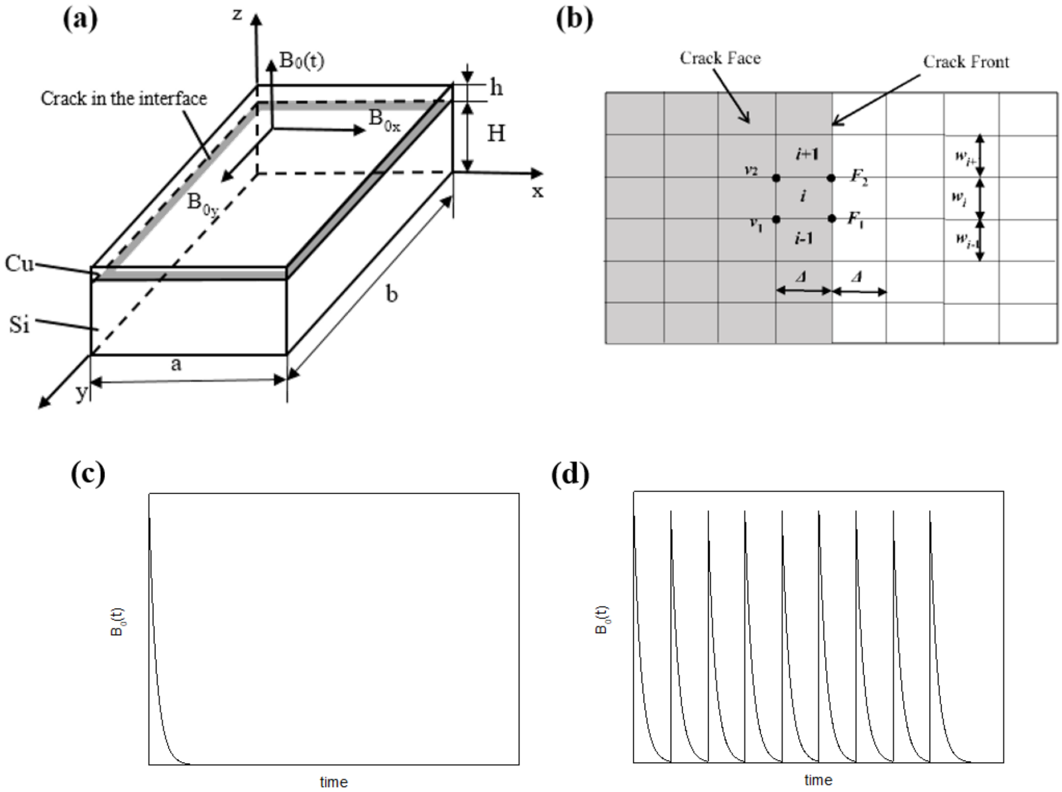

Fig. 1. Schematic drawings of silicon/copper thin plate (a) and the model for the virtual crack closure technique (VCCT) (b). The single-pulsed (c) and multi-pulsed (d) magnetic fields vary with time.

2.1 Equations of Motion

Suppose that a bilayer plate consists of a top metallic layer and a bottom semiconductor layer, representing a simplified multilayer structure ubiquitous in modern electronic systems [12, 29]. This bilayer thin plate is subjected to a time-dependent transverse magnetic field $B_0(t)$ and the in-plane magnetic fields B_{0x} and B_{0y} with fixed values, as shown in Fig. 1(a). The equation of motion of the thin plate can be written as

$$\left[\sigma_{ik}\left(\delta_{jk}+u_{j,k}\right)\right]_{,i}+f_j=\rho\ddot{u}_j \tag{1}$$

where σ_{ij}, u_i, ρ, and f_i are the stress, displacement, density, and external force, respectively. The external force originates from the external magnetic fields, as shown in Fig. 1(a). Using the Kirochoff thin-plate assumption, the equations of motion can be reformulated into a set of geometrical nonlinear differential equations, expressed as [19]:

$$\frac{\partial N_{xx}}{\partial x}+\frac{\partial N_{xy}}{\partial y}+F_x\left(x,y,t\right)=\rho h\frac{\partial^2 u}{\partial t^2} \tag{2}$$

$$\frac{\partial N_{yy}}{\partial y}+\frac{\partial N_{xy}}{\partial x}+F_y\left(x,y,t\right)=\rho h\frac{\partial^2 v}{\partial t^2} \tag{3}$$

$$\begin{aligned}&-D\nabla^2\nabla^2 w-\frac{\alpha Y}{1-\mu}\int_{-h/2}^{h/2}\nabla^2\bar{\theta}z dz+\left(N_{xx}\frac{\partial^2 w}{\partial x^2}+2N_{xy}\frac{\partial^2 w}{\partial x\partial y}+N_{yy}\frac{\partial^2 w}{\partial y^2}\right)\\&+\left(\frac{\partial N_{xx}}{\partial x}+\frac{\partial N_{xy}}{\partial y}\right)\frac{\partial w}{\partial x}+\left(\frac{\partial N_{yy}}{\partial y}+\frac{\partial N_{xy}}{\partial x}\right)\frac{\partial w}{\partial y}+F_z=\rho h\frac{\partial^2 w}{\partial t^2}\end{aligned} \tag{4}$$

where h is the thickness of the thin plate, and u, v, w the displacements along the x-, y- and z-directions, respectively. $D=Yh^3/12\left(1-\mu^2\right)$ is the bending stiffness, with Y and μ being Young's modulus and Poisson's ratio, respectively. α is the thermal expansion coefficient of thin material, $\bar{\theta}$ denotes the temperature change, and N_{xx}, N_{yy}, and N_{xy} the mid-plane resultant forces, defined as $N_{ij}=\int_h \sigma_{ij}dz$. In the above equations (2-4), the external load $\boldsymbol{F}$ (={F_x, F_y, F_z}) is the Lorentz force due to the interactions between electric currents and magnetic fields, which is given by:

$$\boldsymbol{F}=F_x\boldsymbol{i}+F_y\boldsymbol{j}+F_z\boldsymbol{k}=\boldsymbol{J}_\mathbf{e}\times\boldsymbol{B} \tag{5}$$

where $\boldsymbol{J}_\mathbf{e}$ is the eddy current density generated by the transverse magnetic pulse. $\boldsymbol{B}=\boldsymbol{B}_\mathbf{e}+\boldsymbol{B}_\mathbf{0}=B_{ox}\boldsymbol{i}+B_{oy}\boldsymbol{j}+\left(B_0\left(t\right)+B_e\right)\boldsymbol{k}$ is the magnetic field that includes the external magnetic field B_{0x}, B_{0y}, $B_0\left(t\right)$ and the self-inductive $B_e=\mu_0 T$, where μ_0 is the vacuum permeability and T is the component in the $\boldsymbol{k}$-direction of the Eddy current vector.

The finite element formulism of the geometrically nonlinear dynamic governing equation can be derived by Hamilton's principle

$$\delta\int_{t_1}^{t_2}\left(L-\boldsymbol{u}^{\mathrm{T}}\boldsymbol{P}\right)\mathrm{d}x\mathrm{d}y\mathrm{d}t=0 \tag{6}$$

where L is Lagrange function, $\mathbf{u}$ is displacement vector, and $\mathbf{P}$ is the magnetic force vector. Neglecting viscous damping, the Lagrange function can be written as:

$$L=\frac{h}{2}\left(\iint_{\Omega}\rho\left(\frac{\partial\boldsymbol{u}}{\partial t}\right)^{\mathrm{T}}\frac{\partial\boldsymbol{u}}{\partial t}\mathrm{d}x\mathrm{d}y-\iint_{\Omega}\boldsymbol{\varepsilon}^{\mathrm{T}}\boldsymbol{\sigma}\mathrm{d}x\mathrm{d}y\right), \tag{7}$$

where $\boldsymbol{\varepsilon}$ and $\boldsymbol{\sigma}$ are the strain and stress vectors, respectively. One can obtain the dynamic finite element equation as

$$\mathbf{M}_U\left(\frac{\partial^2\mathbf{u}}{\partial t^2}\right)+\mathbf{K}_U\mathbf{u}=\mathbf{R}_U\left(\mathbf{T}\right) \tag{8}$$

At both sides of the interface, nodal displacements must be continuous. One can introduce the penalty function to limit the displacement (in the contact node pair), which is expressed as

$$\left(\boldsymbol{K}_{ca}\right)_e=\bar{\alpha}\boldsymbol{N}_c^{\mathrm{T}}\boldsymbol{N}_c\boldsymbol{u}_c \tag{9}$$

where $\bar{\alpha}$ is the penalty function, $\mathbf{u}_c=\left[\mathbf{u}_1 \quad \mathbf{u}_2\right]^T$ is the displacement of the contacting nodes, $\mathbf{N}_c=\left[\mathbf{I} \quad -\mathbf{I}\right]$, and in other node pairs, $\left(\boldsymbol{K}_{ca}\right)_e=\mathbf{0}$. Using the Gaussian integral and combining Eqs. (6) and (7), and introducing $\boldsymbol{K}_{ca}$ into the finite element equation, one can obtain the multilayer dynamic finite element equation as

$$\mathbf{M}_U\left(\frac{\partial^2\mathbf{u}}{\partial t^2}\right)+\left(\mathbf{K}_U+\mathbf{K}_{ca}\right)\mathbf{u}=\mathbf{R}_U\left(\mathbf{T}\right) \tag{10}$$

where $\mathbf{M}_U = \int_\Omega \rho[N]^T[N]d\Omega$ is the mass matrix, and $[N]$ is the shape function. $\mathbf{R}_U(\mathbf{T}) = \int_\Omega [N][p]d\Omega$ is the external force matrix, which contains the electromagnetic damping force generated by the self-induced magnetic field of thin plates and the equivalent temperature load instead of thermal stress to hinder structural deformation. Here, $[p]$ is the node load. The global stiffness matrix is given as

$$\mathbf{K}_U = \mathbf{K}^{pl} + \mathbf{K}^B + \mathbf{K}^0 = \int_\Omega \left[B^{pl}\right]^T \left[D^{pl}\right]\left[B^{pl}\right] + \left[B^b\right]^T \left[D^b\right]\left[B^b\right] d\Omega + \mathbf{K}^0 \tag{11}$$

where the superscripts *pl* , *b* and *0* mean the in-plane, lateral and nonlinearity terms, respectively. The nonlinearity term introduced by the extra plane strain due to deflection is $\varepsilon^0 = \left\{ \frac{1}{2}\left(\frac{\partial w}{\partial x}\right)^2,\ \frac{1}{2}\left(\frac{\partial w}{\partial y}\right)^2,\ \frac{\partial w}{\partial y}\frac{\partial w}{\partial y} \right\}$. [*B*] is the geometric matrix, and [*D*] is the elastic matrix.

2.2 Electromagnetic Governing Equations

To obtain the Lorentz force ***F***, the current density $\mathbf{J}$ should be determined. Herein, the T-method [19, 40-43] is adopted to solve the generalized Ampere's law based on Maxwell's equations, so as to determine the Eddy current generated under pulsed magnetic fields. Neglecting the electrical displacement and polarization effects, the divergence of the generalized Ampere's law is expressed as:

$$\nabla \cdot \mathbf{J} = 0 \tag{12}$$

Since the thickness of the plate is very small, the Eddy current is considered to be homogenous in the thickness direction. With the introduction of the Eddy current vector $\mathbf{T}$ in the T-method, namely $\boldsymbol{T} = T\boldsymbol{k}$, the Eddy current density can be expressed as:

$$\boldsymbol{J} = J_x \boldsymbol{i} + J_y \boldsymbol{j} = \nabla \times \boldsymbol{T} \tag{13}$$

Where J_x and J_y are the Eddy current densities along the *x*- and *y*-directions, respectively.

The governing equation of Eddy current can be derived from Maxwell's equations. Combining the electromagnetic constitutive relationship with the introduction of the Coulomb gauge condition, Helmholtz's theorems and the Biot-Savart law $\mathbf{B} = \frac{\mu_0}{4\pi}\int_V \frac{\mathbf{J}\times\mathbf{r}}{r^3} dV$ ($\boldsymbol{r}$ is the position vector), the governing equation of Eddy current is expressed as:

$$\frac{\nabla^2 T}{R_*} - \mu_0 \frac{\partial T}{\partial t} = \frac{\partial B_0(t)}{\partial t} - \left(B_{0x} \frac{\partial^2 w}{\partial x \partial t} + B_{0y} \frac{\partial^2 w}{\partial y \partial t} \right) \tag{14}$$

where μ_0 is the vacuum permeability, w is the deflection, $R_*(* = m, s)$ is the electrical resistance, and the subscripts m and s denote the metal and semiconductor layers, respectively. The electrical resistance of semiconductor is denoted as $R_s = 1/\left[e\left(\mu_n n_e + \mu_p p_h \right) \right]$, where e, μ_n, μ_p, n_e and p_h are the charge of an electron, electron mobility, hole mobility, electron concentration, and hole concentration, respectively. The electromagnetic boundary condition is given as $n \times T = 0$, which denotes no normal current component on the boundaries. It is noted that the terms in the parentheses on the right-hand side of Eq. (14) are the electro-mechanical coupling terms.

In order to employ the finite element method to solve Eq. (14) numerically, the Galerkin method is employed with the weight function $\delta\psi = \sum_{i=1}^{n} N_i \delta\psi_i = [N]_e \delta[\psi]_e = \delta[\psi]_e^T [N]_e^T$, which renders the weak form as:

$$\int_{\Omega}\{-\left(\frac{\partial T}{\partial x}\frac{\partial\delta\psi}{\partial t}+\frac{\partial T}{\partial y}\frac{\partial\delta\psi}{\partial y}\right)/R_{*}-\mu_{0}\frac{\partial T}{\partial t} -\left[\frac{\partial B_{0}(t)}{\partial t}-B_{0x}\frac{\partial^{2}w}{\partial x\partial t}-B_{0y}\frac{\partial^{2}w}{\partial y\partial t}\right]\}\delta\psi\mathrm{d}\Omega+\int_{\partial\Omega}n\cdot\nabla T\delta\psi\mathrm{d}S=0 \tag{15}$$

Extracting $\delta\psi_j$ from Eq. (15) and assuming constant T at the boundary $\partial\Omega$, Eq. (15) is recast as:

$$\delta[\psi]_e\int_{\Omega}\left\{-\left(\frac{\partial[N]_e}{\partial x}\frac{\partial[N]_e}{\partial t}+\frac{\partial[N]_e}{\partial y}\frac{\partial[N]_e}{\partial y}\right)[T]_e/R_{*}-\mu_{0}\frac{\partial[N]_e}{\partial t}[N]_e[T]_e\right\}\mathrm{d}\Omega =\delta[\psi]_e\int_{\Omega}\left\{-\left[\frac{\partial B_{0}(t)}{\partial t}-B_{0x}\frac{\partial^{2}w}{\partial x\partial t}-B_{0y}\frac{\partial^{2}w}{\partial y\partial t}\right][N]_e\right\}\mathrm{d}\Omega \tag{16}$$

where $[T]_e$ is the Eddy current vector on the nodes. Based on Eq. (16), the distribution of the Eddy current vector $\boldsymbol{T}$ can be solved based on the following finite element form:

$$\boldsymbol{K}_E\boldsymbol{T}-\boldsymbol{P}_E\frac{\partial\boldsymbol{T}}{\partial t}=\boldsymbol{F}_E\left(B_0(t),w\right) \tag{17}$$

where $\mathbf{K}_E=\int_{\Omega}\left(\frac{\partial[N]_e^T}{\partial x}\frac{\partial[N]_e}{\partial x}+\frac{\partial[N]_e^T}{\partial y}\frac{\partial[N]_e}{\partial y}\right)/R_{*}d\Omega$ is the electromagnetic stiffness matrix, $\mathbf{P}_E=\int_{\Omega}\mu_0[N]_e^T[N]_e d\Omega$ is the stiffness matrix related to the magnetic flux density induced by Eddy current, and $\boldsymbol{F}\left(B_0(t),w\right)=\int_{\Omega}[N]_e\left(-\frac{\partial B_0(t)}{\partial t}+B_{0x}\frac{\partial^2 w}{\partial x\partial t}+B_{0y}\frac{\partial^2 w}{\partial y\partial t}\right)\mathrm{d}\Omega$ is the load on Eddy current induced by displacement and magnetic field.

2.3 Equations of Heat Conduction and Thermo-elastic Coupling

Since Eddy current leads to Joule heating, Ohm's law is used and the heat source S can be written as

$$S=\int_{\Omega}\mathbf{E}\bullet\mathbf{J}d\Omega=\frac{1}{\sigma_{elec}}J^2 \tag{18}$$

where $\mathbf{E}$ is the electric field intensity, and σ_{elec}=1/R_* is the electric conductivity. The Fourier equation of heat conduction is then given as:

$$\lambda\nabla^2\Theta = c\rho\frac{\partial\Theta}{\partial t} - S \tag{19}$$

where Θ is the temperature, λ the thermal conductivity, and c the specific heat.

The thermal boundaries involve both convective boundary and conduction boundary. The heat flow to the surrounding medium is convective, which can be obtained by the Newton's Law of cooling formula. The conduction boundary lines between the two lays are formulated as:

$$\lambda\frac{\partial\Theta}{\partial n}\bigg|_S = q_{\mathrm{sc}} = \bar{\beta}\left(\Theta_e - \Theta_s\right) \tag{20}$$

$$\lambda\frac{\partial\Theta}{\partial n}\bigg|_S = q_{si} = \left(-1\right)^i\left(\Theta_{metal} - \Theta_{semi}\right)/R_\lambda \quad (i = 1,2) \tag{21}$$

where q_{s1} , q_{S2} and q_{sc} are the heat inflows from metal, semiconductor and environment, respectively, R_λ the thermal contact resistance between the copper and semiconductor layers, $\bar{\beta}$ the convection coefficient, Θ_e the temperature of the surrounding air, Θ_s the temperature of the boundary medium, and Θ_{metal} and Θ_{semi} the metal and semiconductor temperatures of the contact point, respectively.

Supposing that heat conductivities are constant, the variational method is applied to establish the functional formulism to derive the corresponding finite element equation, given as

$$\begin{aligned}\Pi = &\int_{t_1}^{t_2}(\int_\Omega \frac{\lambda}{2}\left(\nabla\Theta\right)^2 - \Theta\left(S - c\rho\frac{\partial\Theta}{\partial t}\right)\mathrm{d}\Omega \\ &+\int_S \beta\left(\frac{1}{2}{\Theta_s}^2 - \Theta_e\Theta_s\right) + \Theta_s\left(-1\right)^i\left(\frac{1}{2}\Theta_{\mathrm{metal}} - \Theta_{\mathrm{semi}}\right)/R_\lambda dS)\mathrm{d}t\end{aligned} \tag{22}$$

Through the variational operation and taking $\delta\Pi = 0$, the finite element equation of heat conduction can be written as

$$\boldsymbol{C}_T \frac{\partial \Theta}{\partial t} + \boldsymbol{K}_T \Theta = \boldsymbol{R}_T \tag{23}$$

where $\mathbf{C}_T$ is the specific heat matrix, $\mathbf{K}_T$ is the thermal stiffness matrix consisting of heat conduction matrix, convection matrix and contact heat conduction matrix, and $\mathbf{R}_T$ is the internal and external heat source.

Due to the existence of the change of temperature in the plate under pulsed magnetic field, one needs to consider the effect of thermal stress on the deformation and failure behavior. The stress-strain relationship of an isotropic thermo-elastic material can be expressed as

$$\sigma_{ij} = \frac{Y\mu}{(1+\mu)(1-2\mu)}\varepsilon_{kk}\delta_{ij} + \frac{Y}{1+\mu}\varepsilon_{ij} - \frac{Y\alpha_T\bar{\theta}}{1-2\mu}\delta_{ij} \quad (i, j = x, y) \tag{24}$$

where α_T is the thermal expansion coefficient of thin material, and $\bar{\theta} = \Theta_1 - \Theta_0$ denotes the temperature change.

2.4 Failure Criterion of Two-layered Thin Plate

To describe the delamination behavior in the bilayer structure, the virtual crack closure technique (VCCT) proposed by Rybicki and Kanninen [44] is adopted to solve a two-dimensional crack problem. This method has also been extended to solve a three-dimensional crack problem [45]. For the finite element mesh as shown in Fig. 1(b), the energy release rate can be calculated by the principle of virtual work, given as [46]

$$G_i^k = \frac{1}{2\Delta w_i}\sum_{j=1}^{2} C_j F_j^k V_j^k \quad (k = 1, 2, 3) \tag{25}$$

where $G_i\left(i=\mathrm{I,II,III}\right)$ is the energy release rate of different fracture modes, V_j^k is the displacement of the first node behind the crack front between a delaminated layer, F_j the nodal force at the crack front, w_i the width of the element, Δ the length of the element, and k the different crack mode. Constants C_j are given by

$$C_1=\frac{w_i}{w_{i-1}+w_i},C_2=\frac{w_i}{w_i+w_{i+1}} \tag{26}$$

For the sake of determining the crack propagation, the criterion of crack propagation must be specified. The power-law criterion is widely applied to predict delamination propagation under mixed-mode fracture conditions [47, 48], the formula for this criterion can be expressed as

$$\left(\frac{G_{\mathrm{I}}}{G_C}\right)^{\alpha}+\left(\frac{G_{\mathrm{II}}}{G_C}\right)^{\beta}+\left(\frac{G_{\mathrm{III}}}{G_C}\right)^{\chi}\geq 1 \tag{27}$$

where α, β and χ are constants, which denote the contribution of different crack modes to crack propagation. Crack propagation occurs when the value of the left side of Eq. (27) is greater than 1.

3 Results and Discussion

To explore the multi-field coupling behavior of the bilayer thin plate under magnetic fields as shown in Fig. 1(a), numerical simulation based on the proposed governing equations has been carried out with the physical and geometrical parameters listed in Table 1. The mechanical response and damage behavior of the rectangular bilayer plate under a single transverse magnetic pulse $B_0\left(t\right)=B_{0z}e^{-t/\tau}$, as seen in Fig. 1(c), is studied first, where the magnetic pulse parameter $\tau=10^{-5}s$. Herein, the in-plane magnetic fields are $B_{0x}=B_{0y}=0.6T$. The boundary of the silicon layer perpendicular to the *x*-direction is fixed, and the other boundary is free. The copper layer bonded to the silicon layer is free. So the Si layer can move along the *x*- and *y*-directions, but the Cu layer is limited by the Si layer. A crack is prescribed at the boundary of the interface with a size of one node as 0.0038 m to explore the failure behavior under the electromagnetic fields. This initial crack may represent interfacial defects that are inevitable in a deposition process.

Table 1. The geometric and physical parameters of two-layered thin plate

Parameter	Silicon layer	Copper layer
Length a	0.05 m	0.05 m
Width b	0.05 m	0.05 m
Height h	10^{-4} m	10^{-5} m
Young's modulus Y	180 GPa	120 GPa
Poisson's ratio μ	0.2	0.34
Density ρ	2.329 g/cm^3	8.96 g/cm^3
Electric conductivity σ	2500 S/m	5.959×10^{7} S/m
Permeability μ_0	1.26×10^{-6} H/m	1.26×10^{-6} H/m
Thermal expansion coefficient α	2.6×10^{-6} K^{-1}	1.65×10^{-6} K^{-1}
Thermal conductivity λ	149 W/mK	401 W/mK
Convection coefficient β	50 W/m^{2}K	50 W/m^{2}K
Specific heat density $c\rho$	0.2 J/m^{3}K	0.34 J/m^{3}K
Thermal contact resistance R_λ	2×10^{-4} m^{2}K/W	2×10^{-4} m^{2}K/W

Because of the transverse pulsed magnetic field, the Eddy currents arise in layered plate. Taking the case of Si layer as an example in Fig. 2(a), the current increases from the center of the plate to the perimeters, and the maximum Eddy current is at the midpoint of an edge. Figure 2(b) shows the temperature distribution in the Si layer, and the temperature at the edge is higher than that at the center owing to the corresponding distributed Eddy currents. With the generation of Eddy currents, the interaction of current and magnetic fields results in the appearance of the Lorentz force. The in-plane Lorentz forces in the Si layer are plotted in Fig. 2(c). It is interesting to note that the Lorentz force is compressive, and the force also increases from the center to the edge. Similar distributions of Eddy currents, temperature and Lorentz force can be found in the copper layer. Figure 2(d) shows how the Eddy current density varies with time at the point (0, b/2) in the silicon layer and the copper layer. It is noted that the Eddy current increases with the increase of the intensity of the pulsed magnetic field. Because the conductivity of silicon is smaller than that of copper, the Eddy current generated in the silicon layer under the pulsed magnetic field is much smaller than that in the copper layer. Compared with the large Eddy current in the copper layer, the Eddy current in the silicon layer is much smaller. It is interesting to note that the Eddy current in silicon shows a periodic fluctuation when the magnetic field is weakened. This results from the interaction between the magnetic field and the oscillations of the plate caused by the large Eddy current at the beginning. Figure 2(e) compares the Lorentz forces in the two layers at the point (0, b/2), which corresponds to the change of the Eddy current. Note that the in-plane Lorentz force in the copper layer is much larger than that in the silicon layer, which could lead to delamination. Based on the VCCT described in Subsection 2.4, the energy release rate is calculated and the ratio of the maximum energy release rate to the critical value [46] is shown in Fig. 2(f). With the increase in the strength of the magnetic field, the energy release rate increases but still remains far from the critical value of damage. It means that the bilayer thin plate can keep safe under the single-pulsed magnetic field.

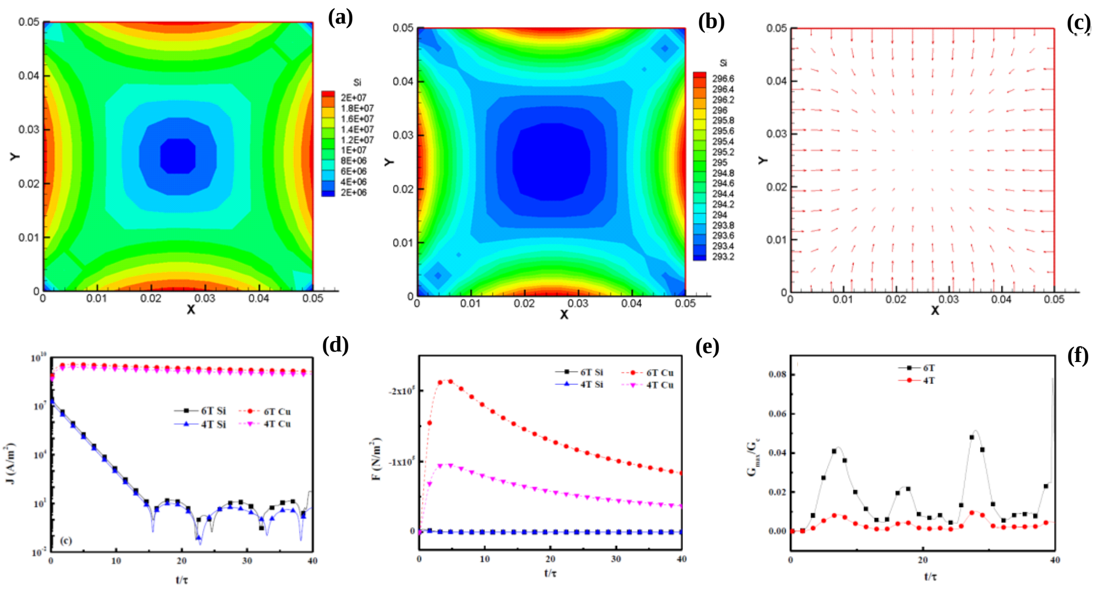

Fig. 2. The Eddy current density distribution (a), the temperature distribution (b), and the in-plane Lorenz force distribution (c) in the Si layer of the bilayer thin plate under a single-pulsed magnetic field; the variations of Eddy current density (d) and Lorenz force (e) with time at point (0, b/2) in the Si and Cu layers under different magnetic strengths, and the energy release rate under different magnetic strengths (f).

We further consider the case of multiple magnetic pulses with the form of $B_0(t)=\sum_{i=0}^{n\text{-}1} B_{0z}\mathrm{e}^{-(t-it_0)/\tau}H(t-it_0)$, where $H(t-it_0)$ is the step function, $t_0=5\times10^{-5}\mathrm{s}$, $n=9$, as seen in Fig. 1(d). Other conditions remain the same as the previous case of single-pulsed magnetic field. Figures 3(a) and 3(b) depict the variations of Lorentz force and energy release rate at the critical point (0, b/2) under different magnetic strengths B_{0z}, respectively. Under multiple magnetic pulses, the current density in the Cu layer keeps a high magnitude, while the current in the Si layer is small. The large and stable Eddy current in the Cu layer enhances the in-plane Lorentz force, while the latter in the Si layer remains small, whose periodic behavior is the same as the Eddy current (although the Y-axis adopts a different scale type), as shown in Fig. 3(a). As a result, the energy release rate rises rapidly and approaches the critical value of delamination, as shown in Fig. 3(b). When delamination occurs, the copper layer undergoes a large lateral displacement under the Lorentz force, leading to crack propagation in the two-layered structure. Note that the Eddy current and the related in-plane force are sensitive to the physical parameters of the applied pulsed magnetic field, such as the strength B_{0z} and the characteristic time τ; as a result, the damage behavior of bilayer thin plate could be dependent on these parameters. Therefore, the critical values of these parameters for the delamination behavior in the bilayer can be obtained through simulations. Figures 3(c) and 3(d) exemplify the variations of the starting time of damage against B_{0z} and τ, respectively. It is noted from the figure that the starting time of damage decreases with B_{0z} but increases with τ. When B_{0z} and τ are smaller than certain values, the delamination of the thin plate would not occur. In application, it means the critical region in the parametric space of pulsed magnetic field, wherein the bilayer thin plate is free from delamination.

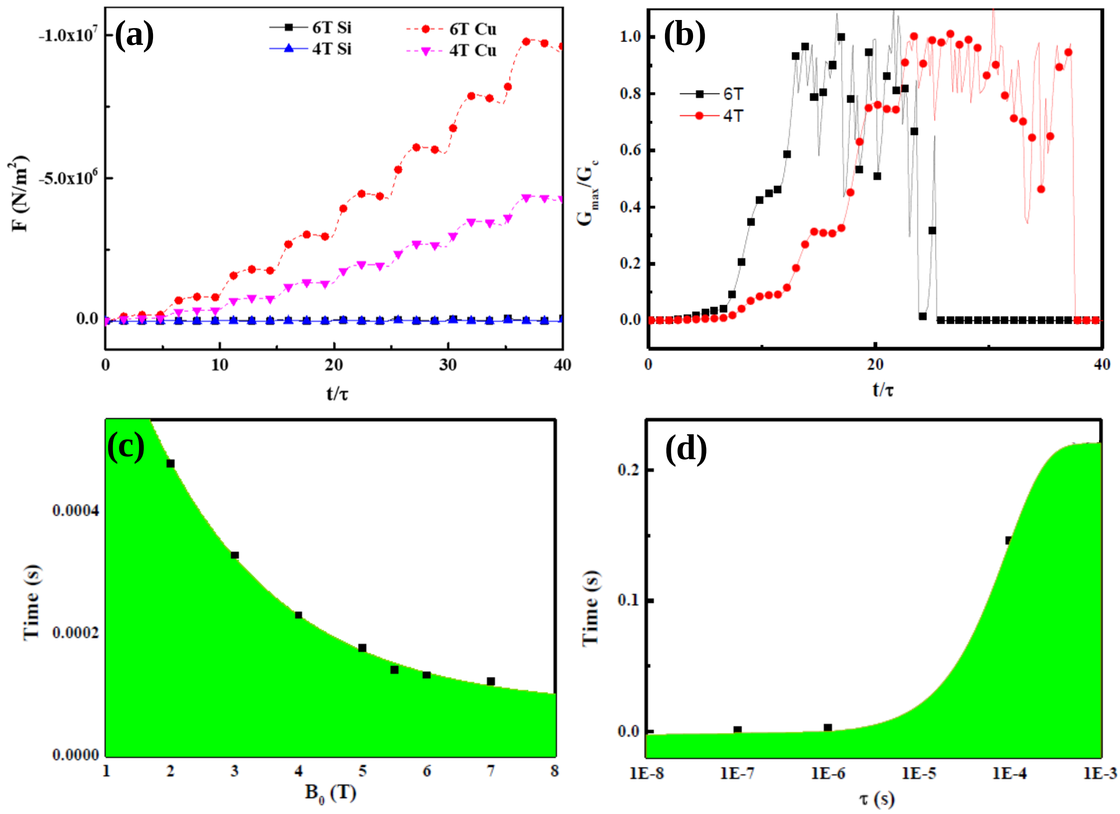

Fig. 3. The variations of in-plane Lorenz force (a) and energy release rate (b) with time for different magnetic fields. The time from the incident of magnetic pulse to delamination versus the magnetic strength with $\tau = 10^{-5}$ (c) and the pulse duration τ with B_{0z} = 6T (d).

4 Conclusion

In summary, the electromagnetic-thermo-mechanical coupling behaviors of Cu/Si thin plate under pulsed magnetic fields are investigated theoretically. The finite element method is employed to solve the governing equations and determine the distributions of Eddy current, temperature and in-plane Lorentz force in each layer of the thin plate and the possibility of delamination. Simulation results demonstrate that under multiple pulses, the accumulation of current in the copper layer leads to significantly different temperature and Lorenz force between Cu and Si layers, which can cause delamination of the two layers. The high temperature in the Cu layer could also impair the performance of the electronic devices. Under magnetic pulses, the time to delamination can be determined using the numerical model. The threshold strength and duration of magnetic pulses, which does not deteriorate the integrity of a multilayer system, would be useful for the design and performance evaluation of the electronic devices applied under strong electromagnetic pulses.

Acknowledgement

This research is supported by the National Natural Science Foundation of China (Grant nos. 11772294, 11621062), and the Fundamental Research Funds for the Central Universities (Grant no. 2017QNA4031).

Conflict of interest

On behalf of all authors, the corresponding author states that there is no conflict of interest.

References

[1] Klyuchnik A V, Pirogov Y A, Solodov A V. Investigation of the IC resistance to pulsed electromagnetic radiation. Journal of Communications Technology and Electronics 2011; 56(3): 342-346.

[2] Giles J C, Prather W D. Worldwide high-altitude nuclear electromagnetic pulse simulators. IEEE Transactions on Electromagnetic Compatibility 2013; 55(3): 475-483.

[3] Chakarothai J, Watanabe S, Wake K. Numerical dosimetry of electro-magnetic pulse exposures using FDTD method. IEEE Transactions on Antennas and Propagation 2018; 66 (10): 5397-5408.

[4] Li GJ, Amer N , Hafez HA , Huang SH , Turchinovich D , Mochain VN, Hegmann FA, Titova LV. Dynamical control over terahertz electromagnetic interference shielding with 2D Ti3C2Ty mxene by ultrafast optical pulses. Nano Letters 2020; 20(1): 636-643.

[5] Yeong-Kook Oh, W.C. Kim, K.R. Park, et al. Commissioning and initial operation of KSTAR superconducting tokamak. Fusion Engineering and Design 2009;84;344-350.

[6] Shimomura Y. Overview of International Thermonuclear Experimental Reactor (ITER) engineering design activities. Physics of Plasmas 1994;1;1612-1618

[7] Radasky W A, Baum C E, Wik M W. Introduction to the special issue on high-power electromagnetics and intentional electromagnetic interference. IEEE Transactions on Electromagnetic Compatibility 2004; 46(3): 314-321.

[8] Shurenkov VV, Pershenkov VS. Electromagnetic pulse effects and damage mechanism on the semiconductor electronics. FACTA Universitatis-Series Electronics and Energetics 2016; 29(4): 621-629.

[9] Baek J E, Cho Y M, Ko K C. Analysis of design parameters reducing the damage rate of low-noise amplifiers affected by high-power electromagnetic pulses. IEEE Transactions on Plasma Science 2018; 46(3): 524-529.

[10] Lee K, Ko K. Propagation model of high-power electromagnetic pulse by using a

serial-parallel resistors circuit. IEEE Transactions on Plasma Science 2014; 42 (10): 3309-3312.

[11] Deng F X, Cao Q L, Han X T, Chen Q, Li L. Principle and realization of an electromagnetic pulse welding system with a dual-stage coil. International Journal of Applied Electromagnetics and Mechanics 2018; 57 (4): 389-398.

[12] Jin J M, Yan S. Multiphysics modeling in electromagnetics. IEEE Antennas Propagation Magazine 2019; 61(2): 14-26.

[13] Tavakoli M H, Karbaschi H, Samavat F. Computational study of electromagnetic fields, eddy currents and induction heating in thin and thick work pieces. Communications in Computational Physics 2010; 8 (1): 211-225.

[14] Karimi M, Shahidi A R. Bending and buckling analyses of BiTiO3–CoFe2O4 nanoplates based on nonlocal strain gradient and modified couple stress hypotheses: rate of surface layers variations. Appl. Phys. A 2019; 125: 530.

[15] Stampfli R, Youssef G. Multiphysics computational analysis of multiferroic composite ring structures. International Journal of Mechanical Sciences 2020; 177: 105573.

[16] Horie T, Niho T. Electromagnetic and structural coupled analysis with the effect of large deflection. IEEE Transactions on Magnetics 1997; 33(2): 1658-1661.

[17] Tanaka Y, Horie T, Niho T. Simplified analysis method for vibration of fusion reactor components with magnetic damping. Fusion Engineering and Design 2000; 51: 263-271.

[18] Hu YD, Li J. Magneto-elastic combination resonances analysis of current-

conducting thin plate. Appl Math Mech-Engl Ed 2008; 29(8): 1053-1066.

[19] Zhang J P, Yan Z J, Ding Q F, Wu H, Pan W G.Analysis of magnetoelastic interaction of cantilever conductive thin plate with nonlinear dynamic response. European Journal of Mechanics-A/Solids 2013; 37:132-138.

[20] Ghayesh M H, Farokhi H, Alici G. Size-dependent electro-elasto-mechanics of MEMS with initially curved deformable electrodes. International Journal of Mechanical Sciences 2015; 103: 247-264.

[21] Liu Y, Chai C C, Yang Y T, et al. Damage effect and mechanism of the GaAs high electron mobility transistor induced by high power microwave. Chinese Physics B 2016; 25(4): 048503.

[22] Lu T J, Jin J M. Coupled electrical-thermal-mechanical simulation for the reliability analysis of large-scale 3-D interconnects. IEEE Trans Compon Pack Manuf Technol 2017; 7(2): 229-237.

[23] Lu T J, Jin J M. Electrical-thermal co-simulation for analysis of high-power RF/microwave components. IEEE Transactions on Electromagnetic Compatibility 2017; 59(1): 93-102.

[24] Dobykin V D. Dependence of the criterial levels of damage in semiconductor structures under the action of high-power electromagnetic pulse on the pulse rise rate. Journal of Communications Technology and Electronics 2011; 56 (2): 214-219.

[25] Musii R S. Thermal stressed state of conducting cylinders subjected to the electromagnetic action in the mode with pulsed modulating signals. Materials

Science 2015; 50 (4): 496-506.

[26] Liu Y, Chai C, Yu X, Fang Q, Yang Y, Xi X, Liu S. Damage effects and mechanism of the GaN high electron mobility transistor caused by high electromagnetic pulse. ACTA Physica Sinica 2016; 65 (3): 038402.

[27] Dobykin V, Kharchenko V. Electromagnetic-pulse functional damage of semiconductor devices modeled using temperature gradients as boundary conditions. Journal of Communications Technology and Electronics 2006; 51(2): 231-239.

[28] Ren Z, Yin W Y, Shi Y B, Liu Q H. Thermal accumulation effects on the transient temperature responses in LDMOSFETs under the impact of a periodic electromagnetic pulse. IEEE Trans Electron Devices 2010; 57(1): 345-352.

[29] Zhou W F, Zhou L, Lin L, Yin W Y, Mao J F. Electrothermal-stress interactions of LDMOS FET induced by DCI RF-pulses. IEEE Transactions on Electromagnetic Compatibility 2014; 56(5): 1178-1184.

[30] Zhou L, Yin W Y, Zhou W F, Lin L. Experimental Investigation and Analysis of the LDMOS FET Breakdown Under HPM Pulses. IEEE Transactions on Electromagnetic Compatibility 2013; 55(5): 909-916

[31] Zhou L, San Z W, Hua Y J, Lin L, Zhang S, Zhao Z G, Zhou H J, Yin W Y. Investigation on Failure Mechanisms of GaN HEMT Caused by High-Power Microwave (HPM) Pulses. IEEE Transactions on Electromagnetic Compatibility 2017; 59(3): 902-909.

[32]C. Zhang, R. Zhang, T. Yan, Z. Yang, W. Ren and Z. Zhu, A 3D theoretical model

for EMP thermal runaway in semiconductor devices, 2019 International Conference on Electromagnetics in Advanced Applications (ICEAA), 2019, 1156-1159.

[33]Y. Li, H. Xie, H. Yan, J. Wang and Z. Yang, "A Thermal Failure Model for MOSFETs Under Repetitive Electromagnetic Pulses," IEEE Access 2020; 8: 228245-228254.

[34] Camp M, Gerth H, Garbe H, Haase, H. Predicting the breakdown behavior of microcontrollers under EMP/UWB impact using a statistical analysis. IEEE Transactions on Electromagnetic Compatibility 2004; 46(3): 368-379.

[35] Xi X W, Chai C C, Ren X R, Yang Y T, Zhang B, Hong X. EMP injection damage effects of a bipolar transistor and its relationship between the injecting voltage and energy. Journal of Semiconductors 2010; 31(4): 044005.

[36] Ma Z Y, Chai C C, Ren X R, Yang Y T, Chen B, Song K, Zhao Y B. Microwave damage susceptibility trend of a bipolar transistor as a function of frequency. Chinese Physics B 2012; 21(9): 098502.

[37] Genender E, Garbe H, Sabath F. Probabilistic Risk Analysis Technique of Intentional Electromagnetic Interference at System Level. IEEE Transactions on Electromagnetic Compatibility 2014; 56(1): 200-207.

[38] Shurenkov V V, Pershenkov V S. Electromagnetic pulse effects and damage mechanism on the semiconductor electronics. Facta Universitatis, Series: Electronics and Energetics 2016; 29(4): 621-629.

[39]J. Baek, Y. Cho and K. Ko, Analysis of Design Parameters Reducing the Damage

Rate of Low-Noise Amplifiers Affected by High-Power Electromagnetic Pulses,IEEE Transactions on Plasma Science 2018; 46(3): 524-529.

[40] Gao Y, Xu B, Huh H. Electromagneto-thermo-mechanical behaviors of conductive circular plate subject to time-dependent magnetic fields. Acta Mechanica 2010; 210(1-2): 99-116.

[41] Grilli F, Pardo E, Stenvall A, Nguyen D N, Yuan W, Gomory F. Computation of losses in HTS under the action of varying magnetic fields and currents. IEEE Transactions on Applied Superconductivity 2014; 24(1): 78-110.

[42] Takagi T, Hashimoto M, Arita S, Norimatsu S, Sugiura T & Miya K. Experimental verification of 3D eddy current analysis code using T-method. IEEE Transactions on Magnetics 1990; 26(2), 474-477.

[43] Zheng X J, Zhang J P, Zhou Y H. Dynamic stability of a cantilever conductive plate in transverse impulsive magnetic field. International Journal of Solids Structures 2005; 42: 2417-2430.

[44] Rybicki E F, Kanninen M F. A finite element calculation of stress intensity factors by a modified crack closure integral. Engineering Fracture Mechanics 1977; 9(4): 931-938.

[45] Shivakumar K, Tan P, Newman J. A virtual crack-closure technique for calculating stress intensity factors for cracked three dimensional bodies. International Journal of Fracture 1988; 36(3): R43-R50.

[46] Bagchi A, Evans A G. The mechanics and physics of thin film decohesion and its measurement. Interface Science 1996; 3(3): 169-193.

[47] Chang-Chun Lee. Overview of interfacial fracture energy predictions for stacked thin films using a four-point bending framework, Surface & Coatings Technology 2013;237:333–340.

[48] Guotao Wang, C. Merrill, Jie-Hua Zhao, S. K. Groothuis and P. S. Ho, Packaging effects on reliability of Cu/low-k interconnects. IEEE Transactions on Device and Materials Reliability 2003;3(4):119-128